Analogue Cosmology with 2-fluid systems in a strong gradient magnetic field

Zack Fifer,[1, 2] Theo Torres,[1, 2] Sebastian Erne,[1, 2] Anastasios
Avgoustidis,[3] Richard J. A. Hill,[3] and Silke Weinfurtner[1, 2]

[1] *School of Mathematical Sciences, University of Nottingham, University Park, Nottingham NG7 2RD, UK*
[2] *Centre for the Mathematics and Theoretical Physics of Quantum Non-Equilibrium Systems,*
University of Nottingham, Nottingham NG7 2RD, UK
[3] *School of Physics and Astronomy, University of Nottingham, Nottingham NG7 2RD, UK*

We propose a novel experiment combining fluid dynamics and strong magnetic field physics to simulate cosmological scenarios. Our proposed system consists of two immiscible, weakly magnetised fluids moved through a strong gradient magnetic field. The diamagnetic and paramagnetic forces thus generated amount to a time-dependent effective gravity, which allows us to precisely control the propagation speed of interface waves. Perturbations on the interface therefore experience a nonstationary effective metric. In what follows, we demonstrate that our proposed system is capable of simulating a variety of cosmological models. We then present a readily realisable experimental setup which will allow us to capture the essential dynamics of standard inflation, wherein interface perturbations experience a shrinking effective horizon and are shown to transition from oscillatory to frozen and squeezed regimes at horizon crossing.

The physics of the early universe is deeply linked to drastic changes in spacetime geometry. In the standard scenario the primordial universe expanded in a nearly exponential fashion, a phase known as inflation [1]. Rival models to inflation include cyclic or ekpyrotic scenarios [2–7], while for earlier epochs even more exotic scenarios have been proposed, involving transitions from a Lorentzian to a Euclidian signature in the spacetime metric [8–13]. Since these scenarios could have only been realised at the very earliest periods in the evolution of our universe – corresponding to energy scales unattainable in a laboratory experiment – we do not have direct experimental access to their fascinating physics. Instead, only their low-energy remnants can be observed and experimentally tested against theoretical predictions. As we will argue in this letter, analogue simulators capable of mimicking some of the elusive early universe processes may offer an alternative avenue of investigation.

Pioneered by Unruh [14], analogue gravity setups focusing mainly on effects arising from black hole spacetime geometries [15–21] have offered the possibility to recreate fundamental effects such as Hawking radiation or superradiance. Experimental investigations in realistic laboratory setups have resulted in a deeper understanding of these effects beyond their original domain of applicability [22–28] and brought to light the strength of analogue gravity. Extending the analogy, superfluids have allowed the study of time-dependent spacetime geometries, both theoretically [29–34] and experimentally [35, 36]. Building upon recent successes of analogue gravity experiments using water-waves, we propose the first classical fluid system to mimic wave-propagation in time-dependent spacetimes.

We consider perturbations on the interface between two immiscible liquids, a diamagnetic layer lying atop a paramagnetic one, that can be moved at a precisely controllable rate through a strong, spatially varying magnetic field $B(\vec{x}, t)$ generated by a superconducting solenoid or a Bitter magnet (c.f. Ref. [37, 38]). The combined magnetic and gravitational body forces applied to the liquid sample amount to an effective gravitational force, which can be used to render the propagation speed c of the interfacial perturbations time dependent. The corresponding analogue metric in our system $g_{\mu\nu} \propto \text{diag}(-c(t)^2, 1, 1)$ can thereby be taylored to represent a variety of early universe cosmological scenarios, such as inflation, cyclic universes, bounces, and signature change events.

After a theoretical discussion of the system, we present in detail our proposed experimental implementation and compare, as a first example, explicit results in the linear (dynamic) regime of a simulated experimental setup with results for inflationary dynamics. Apart from demonstrating the possibility for direct experimental investigations of fundamental effects such as mode freezing and quasi-particle production, our analogue system shows the opportunity to provide insight into field dynamics at the earliest times of our Universe through experiments in a laboratory setup.

Two-fluid systems.—We consider an immiscible two-fluid system (Fig. 1), with densities $\rho_1 > \rho_2$, heights $h_{1,2}$, small magnetic susceptibilities $|\chi_{1,2}| \ll 1$, and flow velocities $v_{1,2}$. The system is subjected to a magnetic field $B(\vec{x}, t)$ with a large vertical gradient. The flow of an inviscid and incompressible fluid is described by the continuity equation and Euler's momentum equation with the inclusion of the magnetic potential energy [39, 40]:

$$\vec{\nabla} \cdot \vec{v}_i = 0 \tag{1}$$

$$\rho_i \left(\partial_t + \vec{v}_i \cdot \vec{\nabla} \right) \vec{v}_i = \vec{\nabla} \left(-p_i + \frac{\chi_i}{2\mu_0} B^2 \right) + \rho_i \vec{g} . \tag{2}$$

The index $i = 1$ ($i = 2$) labels the lower (upper) fluid, p_i is the fluid pressure, μ_0 the vacuum permeability, and
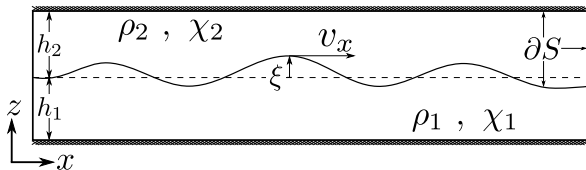
Figure 1. Schematics of the two-liquid system. Two immiscible liquids, with densities $\rho_{1,2}$, magnetic susceptibility $\chi_{1,2}$, and height $h_{1,2}$, separated by the equilibrium interface at z_0 (dotted line). Gravity interface waves distort the interface layer (solid line) where each point is characterized by its amplitude ξ and velocity v_x (v_y). ∂S are the boundaries (here depicted for fluid 2) given by a hard wall (upper), an interface boundary (right), and a moving boundary at the interface of the two liquids (lower).

$\vec{g} = (0, 0, -g)$ is the acceleration due to gravity. The kinematic and, in case of a free surface, dynamic boundary conditions are

$$\vec{v}_i \cdot \vec{n} = \vec{V} \cdot \vec{n} \qquad \text{on} \qquad \partial S \qquad (3)$$

$$[p] = \sigma(R_1^{-1} + R_2^{-1}) \, , \qquad (4)$$

on a boundary ∂S with velocity $\vec{V}$. Equation (3) states that the velocity of the fluid equals the velocity of the boundary along the outward normal $\vec{n}$ to the boundary. The angled bracket $[*]$ denotes the jump in value across the interface, here the jump in pressure p according to the Young-Laplace law [41] with surface tension σ, and principal radii of curvature $R_{1,2}$.

We assume an irrotational velocity field $\vec{v}_i = \vec{\nabla}\phi_i$, and a liquid-liquid interface ξ given by $z = z_0 + \xi(x, y, t)$. We then linearise Eqs. (1) & (2) around a steady background flow $\vec{v}_0 = \vec{\nabla}\phi_0$ with $\phi_i = \phi_0 + \varphi_i$. We further take $\partial_z B \gg \partial_x B$. At the hard-wall upper and lower boundaries Eqs. (1) & (3) lead to the Ansatz $\varphi_i = \sum_n \cosh[\epsilon_n(z - h_i)]\varphi_{i,n}(x, y, t)$, where n labels the eigenfunctions of the 2D-Laplacian, $(\nabla^2 + \epsilon_n^2)\varphi_n = 0$, on the interface. With the inclusion of magnetic body forces [39, 40], the linear equations of motion obtained by Eqs. (2) – (4) evaluated at the free interface are [41]

$$\rho_1 \mathcal{D}_t \varphi_1 - \rho_2 \mathcal{D}_t \varphi_2 = \left(\sigma \nabla^2 - [\rho]g_0 + \frac{[\chi]}{\mu_0} B \partial_z B \right) \xi \quad (5)$$

$$\mathcal{D}_t \xi = \frac{1}{2} \partial_z (\varphi_1 + \varphi_2) \, , \qquad (6)$$

where the curvature for small deformations ξ is given by $(R_1^{-1} + R_2^{-1}) \simeq -\nabla^2 \xi$ [41] and $\mathcal{D}_t = \partial_t + v_0 \cdot \nabla$ is the material derivative on the 2D interface. While the preceding discussion is valid for arbitrary geometries of the interface, flows, and heights, we now choose a plane wave basis (with wavenumber $n = k$ and $\epsilon_k^2 = k^2$), a vanishing background flow ($\mathcal{D}_t = \partial_t$, depicted with a dot), and equal surface heights $|h_1| = |h_2| \equiv h$.

Since at the interface $v_{1z} = v_{2z}$ (c.f. Eq. (3)), we get

with $\varphi_k \equiv \varphi_{1,k}$

$$\ddot{\varphi}_k + \omega_k^2 \varphi_k = \frac{\dot{G}_k}{G_k} \dot{\varphi}_k \, , \qquad (7)$$

where

$$G_k = \left([\rho]g_{\text{eff}} + \sigma k^2\right) / \tilde{\rho} \, , \qquad (8)$$

with $\tilde{\rho} = \rho_1 + \rho_2$. The left hand side of Eq. (7) describes the familiar oscillatory behaviour with frequency

$$\omega_k^2 = G_k k \tanh(kh) \, . \qquad (9)$$

The effective gravity [42],

$$g_{\text{eff}} = g - \frac{[\chi]}{[\rho]\mu_0} B \partial_z B \, , \qquad (10)$$

is modulated through the spatio-temporal dependence of the external magnetic field $B(\vec{x}, t)$, which introduces an explicit time dependence of the frequency $\omega_k \equiv \omega_k(t)$ as well as an additional friction term (right hand side of Eq. (7)).

Analogue Cosmology.—In order to make the connection with cosmology transparent we consider the shallow water (or long wavelength) limit $kh \ll 1$ (i.e. linearizing the tanh in Eq. (9)). The change in the effective gravity (10) corresponds directly to a change in the propagation speed c_k of long wavelength perturbations. We define the mode-dependent scale factor

$$a_k^{-2}(t) \equiv c_k^2(t) = G_k(t)h \, , \qquad (11)$$

with which the equation of motion (7) takes the form

$$\ddot{\varphi}_k + 2\frac{\dot{a}_k}{a_k}\dot{\varphi}_k + \frac{k^2}{a_k^2}\varphi_k = 0 \, . \qquad (12)$$

Thus, our two fluid system in the shallow water limit is equivalent to a massless scalar field in a Friedmann-Lemaître-Robertson-Walker (FLRW) type rainbow universe [31].

Eqs. (8), (10) and (11) imply that it is possible to change the sign of $a_k(t)^2$ for some, or all, of the modes in the system. Within the analogy, this sign-change corresponds to a Hartle-Hawking-like [12, 13] change from Lorentzian (with a hyperbolic equation of motion) to Euclidian (with an elliptic equation of motion) signature in the analogue spacetime geometry, cf. Eq. (13) below.

The k-dependence in Eq. (11) cannot in general be neglected, even in the long wavelength regime, $k \to 0$, because the magnitude of $[\rho]g_{\text{eff}}$ could approach σk^2 (see Eq. (8)). However, the effect of the surface tension is negligible in the regime $[\rho]g_{\text{eff}} \gg \sigma k^2$. The effective metric for the perturbations then becomes

$$ds^2 = g_{\mu\nu}dx^\mu dx^\nu = -dt^2 + a^2(t)(dx^2 + dy^2) \, , \quad (13)$$

which is the exact FLRW solution to Einstein's equations for an expanding, homogeneous and isotropic universe described by a (k-independent) scale factor $a(t)$.
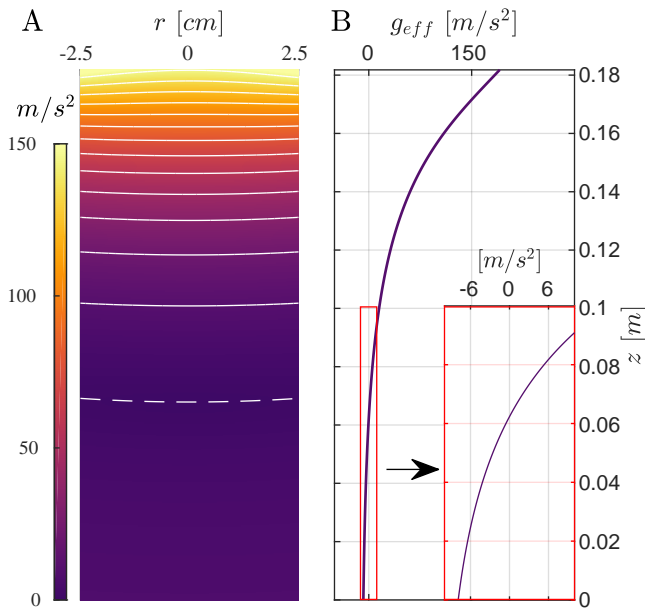
Figure 2. Panel A depicts the effective gravity g_{eff} in the bore of the magnet for the butanol-aqueous solution ($\ddot{z}_0 = 0$). The vertical axis gives the vertical position in the magnet z, and the horizontal axis the radial position r. The magnitude is given by the colorbar. The solid white lines are contours of the effective gravity, with the dashed line depicting the region over which g_{eff} changes sign. Panel B is the effective gravity along the axis of the solenoid ($r = 0$). The inset rescales the horizontal axis to better demonstrate the sign change of g_{eff}.

Experimental implementation.—

We propose experimental studies of a two-liquid system consisting of a layer of butanol lying atop a denser layer of a weak aqueous paramagnetic solution, with a relatively small interfacial surface tension, $\sigma = 1.8\text{mN/m}$ [43] (immiscibility requires $\sigma \neq 0$). The liquids fill completely a transparent toroidal vessel with diameter $d = 4\text{cm}$, designed to fit within the bore of an 18T superconducting solenoid magnet used for magnetic levitation experiments (e.g. [37, 44]). The azimuthal degrees of freedom of perturbations on the annular interface obey periodic boundary conditions, with fundamental wavelength $\lambda_{\text{max}} = \pi d$. The relatively small interfacial tension and maximal wavelength were chosen to minimize non-linear contributions to the dispersion relation.

The versatility of the proposed setup can be seen by considering the experimental parameters in Eq. (8) and Eq. (10). When the vessel is inserted into the solenoid, the effective gravity g_{eff} is altered in general due to a step change in the magnetic susceptibility (see Eq. (10)) across the liquid-liquid interface, and may even be inverted [37, 39, 40, 44]. The effective gravity g_{eff} in the region below the centre of the solenoid is depicted in Fig. 2.

Note the dramatic change in g_{eff} achievable within a

20cm interval. The monotonic relationship between g_{eff} and z_0 allows us to tune the scale factor to mimic the desired cosmological model by controlling the motion of the sample. The time-dependent position and acceleration of the vessel in the magnet is determined by solving the differential equation $g_{\text{eff}}[z_0, \ddot{z}_0] = a_k(t)^2$ (see Fig. 3A). $\ddot{z}_0$ is taken into account by substituting $g \to g + \ddot{z}_0$ in Eq. (10), and $g_{\text{eff}}[z_0, \ddot{z}_0]$ is determined by the physical properties of the fluids, and of the magnet.

The inversion of g_{eff} in our proposed setup allows us to completely nullify the surface tension term σ for a single (long-wavelength) mode in our system. This enables us to produce arbitrarily large expansions as can be seen by calculating the number of e-folds

$$N = \ln\left(\frac{a_k(t_{\text{f}})}{a_k(t_{\text{i}})}\right) = \frac{1}{2}\ln\left(\frac{\sigma k^2 + [\rho]g_{\text{eff}}(t_{\text{i}})}{\sigma k^2 + [\rho]g_{\text{eff}}(t_{\text{f}})}\right), \quad (14)$$

used in cosmology to describe the amount of cosmological expansion.

Explicit results for cosmic Inflation.—

In order to demonstrate that our system is capable of producing the rapid and substantial changes required of cosmological models, we propose a simulation of standard cosmological inflation wherein the scale factor $a(t)$ (c.f. Eq. (13)) in the FLRW metric grows exponentially. In this archetypical model, space expands so quickly that fluctuations are stretched beyond the characteristic scale of the expansion (known as the Hubble horizon), at which point they stop propagating in time (the modes are said to be frozen). By this process small initial perturbations get amplified and converted to density fluctuations, eventually leading to the observed large-scale structure of our universe.

For the experiment, we tune the scale factor $a_k(t)$ to be exponential in the linear dispersion limit. The path through the magnet $z_0(t)$, as well as the acceleration to produce this expansion are shown in Fig. 3A (note the magnitude of $\ddot{z}_0$, as compared to g_{eff} in Fig. 2).

To understand the behavior of the field, it is common to introduce the auxiliary field $\mathcal{X}_k = a_k \varphi_k$ for which the wave equation (7) takes the form of a time-dependent harmonic oscillator with frequency

$$\Omega_k^2(t) = \frac{k^2}{a_k^2} - \frac{\ddot{a}_k}{a_k} . \quad (15)$$

Horizon crossing occurs at $\Omega_k^2 = 0$, separating the oscillating solution dominated by the first term on the right hand side of Eq. (15) from the exponentially growing / decaying solutions at late times, dominated by the time-independent second term. The essence of inflationary dynamics is fully captured for late times after a mode has crossed the horizon, since the dynamics of the physical field φ_k freezes and becomes trivial, obeying a constant solution in time.

Fig. 3B depicts the numerical solution of the field equation (7), including the full non-linear dispersion relation (9), for the longest wavelength of our system. For $t < 0$ the system is evolved in flat space, reducing Eq. (7) to a simple harmonic oscillator. At $t = 0$ the system begins to expand, leading to an oscillatory, damped time evolution of the field. Upon crossing the effective horizon, the field rapidly approaches a nearly constant solution.

The full model (including dispersive effects) exhibits minor differences compared to a completely frozen field solution, caused by the surface tension. The surface tension adds a small time-depence to $\ddot{a}_k/a_k$ and in turn a slow further evolution of the field outside the horizon. Apart from a different effective expansion experienced by high momentum modes, dispersive effects lead to the mode re-entering the Hubble horizon, exhibiting oscillatory behaviour at later times. Nevertheless, our system is able to simulate mode freezing.

We further present the evolution of the surface height $\xi_k = a_k^2 \dot{\varphi}_k$, directly accessible in the experiment through standard interface profilometry methods (see e.g. [45–47]). The surface height exhibits a growing, non-oscillatory solution after horizon crossing. Profilometry measurements provide access to the full evolution of the field, allowing us to observe mode freezing in real time and providing direct evidence for inflationary dynamics of the system.

Our proposed system allows us to stop the expansion and to analyse the inflationary signatures in the resulting flat spacetime through the statistical properties of the state. The associated definition of a well-defined ground state leads to analogue cosmological quasi-particle production, (mode amplification) and two-mode correlations in direct analogy to the squeezed-state formulation of inflation [48, 49]. Mode amplification and correlations are the result of the rapid effective expansion of our analogue universe connecting two flat regions of spacetime $a(t_i) \to a(t_f)$ [50].

In line with field theory in curved spacetime, we introduce the classical quasi-particle amplitudes b_k in the initial flat region of spacetime by expanding the field [51] $\varphi_k(x,t) = \left(f_k^i(t) b_k + f_k^i(t)^* b_{-k}^* \right) \exp(ikx)$ in terms of the time-dependent mode functions (f_k, f_k^*), normalized by the Wronskian $\langle f_k\,;\,f_k \rangle \equiv i\left(f_k^* \partial_t f_k - (\partial_t f_k^*) f_k \right) = 1$. Conservation of the Wronskian implies that the initial and final flat regions of spacetime are related by a Bogoliubov transformation $f_k^i(t) = \alpha_k f_k^f(t) + \beta_k f_{-k}^f(t)^*$, where $|\alpha_k|^2 - |\beta_k|^2 = 1$. The final state is fully described by the corresponding transformation of the amplitudes $d_k \equiv \langle f_k^f(t)\,;\,\varphi_k \rangle = \alpha_k b_k + \beta_k^* b_{-k}^*$. The measurable mode intensity after the effective expansion in our system is

$$\langle d_k^* d_k \rangle = \left(2|\beta_k|^2 + 1 \right) \langle b_k^* b_k \rangle . \tag{16}$$

Here, $\langle \dots \rangle$ denotes the arithmetic mean taken over sufficiently many measurements, allowing us to assume $\langle b_{-k}^* b_{-k} \rangle = \langle b_k^* b_k \rangle$.
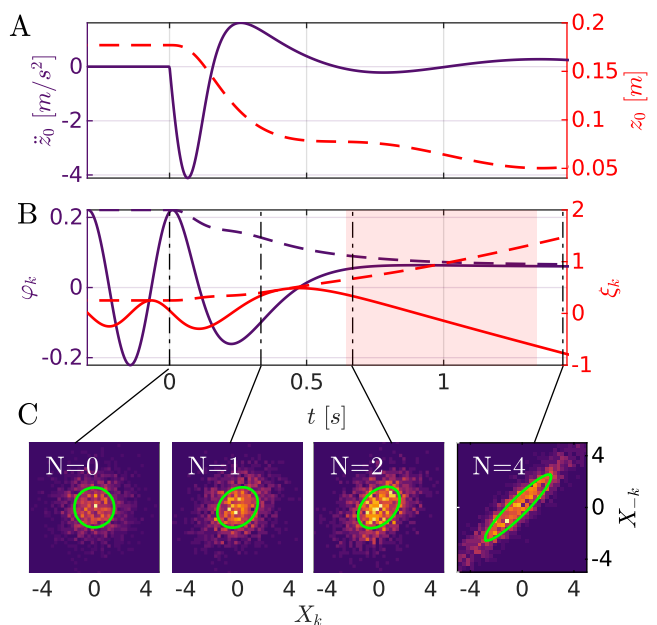

Figure 3. Panel A shows the evolution of the vertical position $z_0(t)$ (dashed red) and acceleration $\ddot{z}_0(t)$ (solid purple) of the vessel in the magnet corresponding to an exponentially inflating analogue universe with Hubble parameter $H = 3\,s^{-1}$. Panel B depicts the solution to the wave equation (12). The solid (dashed) line is the real part (absolute value) of the velocity potential ϕ_k (purple) and of the height field ξ_k (red). The black dash-dotted lines represent different number of e-folds $N = 0, 1, 2$ and 4 for the mode. The shaded region indicates where the mode is outside the Hubble horizon. Panel C depicts the maximal two-mode squeezing of the system projected onto the instantaneous eigenbasis at the times (equivalently number of e-folds) indicated. The solid line indicates the theoretical full width at half maximum for each distribution. The intensity plots represent the probability of a given measurement of X_k and X_{-k} after 2000 simulated experimental runs.

As anticipated from translational invariance in equation (12), the Bogoliubov coefficients α_k, β_k only mix modes of opposite momenta:

$$\langle d_{-k} d_k \rangle = 2\alpha_k \beta_k^* \langle b_k^* b_k \rangle . \tag{17}$$

Wave amplification therefore occurs in the form of correlated, counter-propagating pairs. Defining the variable $X_k = \left(f_k^f(t) d_k + f_k^f(t)^* d_k^* \right)/|f_k^f|$, and the conjugate quadratures $(X_k \pm X_{-k})$, we find from equation Eq. (17) that the variance of a quadrature is lowered below its initial value while the variance of its conjugate is raised so that their product remains constant. Note that while the freezing of the modes is sensitive to $\ddot{a}_k/a_k \approx$ const, creation of counter-propagating pairs is generic (see e.g. [52]).

Fig. 3C shows the build-up of correlations for an initial uncorrelated Gaussian state for varying numbers of e-folds N during the expansion. The maximum squeezing

$|\alpha_k - \beta_k|^2$ caused by the correlations (17) is seen to increase with N (similar behaviour is found by increasing the effective Hubble parameter H). Significant amplification of correlated counter propagating waves occurs once the mode becomes frozen. Note that each mode itself shows no sign of squeezing and is simply amplified according to Eq. (16). By automating the experiment and controlling the initial state, we can sample from a statistical ensemble of analogue universes. This allows us to quantify the impact that deviations from the linear theory will have on our system.

Conclusion.—The precise controllability of the effective metric in our novel system together with the continuous measurement of the field dynamics makes it a versatile tool to explore fundamental questions of wave-dynamics in time-dependent curved spacetimes. This has the potential to elucidate the universality and robustness of characteristic cosmological effects. The validation of our experimental setup on known solutions, such as the proposed inflationary model, allows to transfer the analogy to theoretically less understood models. For example, it would provide an analogue simulator for evolving field fluctuations through bounces and/or signature changes – an open problem in cyclic and pre-big bang models. This work will advance the mutually beneficial interconnection of cosmological and analogue gravity systems.

---

[1] A. H. Guth. The Inflationary Universe: A Possible Solution to the Horizon and Flatness Problems. *Phys. Rev. D*, 23:347–356, 1981.

[2] P. J. Steinhardt and N. Turok. A Cyclic model of the universe. *Science*, 296:1436–1439, 2002.

[3] P. J. Steinhardt and N. Turok. Cosmic evolution in a cyclic universe. *Phys. Rev. D*, 65:126003, 2002.

[4] J. Khoury, B. A. Ovrut, P. J. Steinhardt, and N. Turok. The Ekpyrotic universe: Colliding branes and the origin of the hot big bang. *Phys. Rev. D*, 64:123522, 2001.

[5] J.-L. Lehners. Ekpyrotic and Cyclic Cosmology. *Phys. Rept.*, 465:223–263, 2008.

[6] M. Gasperini and G. Veneziano. The Pre - big bang scenario in string cosmology. *Phys. Rept.*, 373:1–212, 2003.

[7] G. Veneziano. Scale factor duality for classical and quantum strings. *Phys. Lett. B*, 265:287–294, 1991.

[8] S. W. Hawking and I. G. Moss. Supercooled Phase Transitions in the Very Early Universe. *Phys. Lett.*, 110B:35–38, 1982.

[9] A. Vilenkin. Creation of Universes from Nothing. *Phys. Lett.*, 117B:25–28, 1982.

[10] A. Vilenkin. The Birth of Inflationary Universes. *Phys. Rev. D*, 27:2848, 1983.

[11] A. D. Linde. Quantum Creation of the Inflationary Universe. *Lett. Nuovo Cim.*, 39:401–405, 1984.

[12] J. B. Hartle and S. W. Hawking. Wave Function of the Universe. *Phys. Rev. D*, 28:2960–2975, 1983.

[13] J. B. Hartle, S. W. Hawking, and T. Hertog. No-Boundary Measure of the Universe. *Phys. Rev. Lett.*, 100:201301, 2008.

[14] W. G. Unruh. Experimental black hole evaporation. *Phys. Rev. Lett.*, 46:1351–1353, 1981.

[15] Schützhold, Ralf and Unruh, William G. Gravity wave analogues of black holes, *Phys. Rev. D*, 66:044019, Aug 2002.

[16] S. Weinfurtner, E. W. Tedford, M. C. J. Penrice, W. G. Unruh, and G. A. Lawrence. Measurement of stimulated hawking emission in an analogue system. *Phys. Rev. Lett.*, 106:021302, Jan 2011.

[17] F. Belgiorno, S. L. Cacciatori, M. Clerici, V. Gorini, G. Ortenzi, L. Rizzi, E. Rubino, V. G. Sala, and D. Faccio. Hawking radiation from ultrashort laser pulse filaments. *"Phys. Rev. Lett."*, 105(20):203901, 2010.

[18] L.-P. Euvé, F. Michel, R. Parentani, T. G. Philbin, and G Rousseaux. Observation of noise correlated by the hawking effect in a water tank. *"Phys. Rev. Lett."*, 117(12):121301, 2016.

[19] J. Steinhauer. Observation of quantum hawking radiation and its entanglement in an analogue black hole. *Nature Physics*, 12(10):959–965, 2016.

[20] T. Torres, S. Patrick, A. Coutant, M. Richartz, E. W. Tedford, and S. Weinfurtner. Rotational superradiant scattering in a vortex flow. *Nature Physics*, 2017.

[21] D. Vocke, C. Maitland, A. Prain, F. Biancalana, F. Marino, and D. Faccio. Rotating black hole geometries in a two-dimensional photon superfluid. *arXiv preprint, arXiv:1709.04293*, 2017.

[22] S. Corley, T. Jacobson. Hawking spectrum and high frequency dispersion. *Phys. Rev. D*, 54:1568, Jul 1996.

[23] S. Corley. Particle creation via high frequency dispersion. *Phys. Rev. D*, 55:6155, May 1997.

[24] W. G. Unruh, R. Schützhold. Universality of the Hawking effect. *Phys. Rev. D*, 71:024028, Jan 2005.

[25] R. Schützhold and W. G. Unruh. Origin of the particles in black hole evaporation. *Phys. Rev. D*, 78:041504, Aug 2008.

[26] C. Barceló, L. J. Garay, and G. Jannes. Sensitivity of Hawking radiation to superluminal dispersion relations. *Phys. Rev. D*, 79:024016, Jan, 2009.

[27] T. Torres, A. Coutant, S. Dolan, and S. Weinfurtner. Waves on a vortex: rays, rings and resonances. *arXiv preprint, arXiv:1712.04675*, 2017.

[28] S. Patrick, A. Coutant, M. Richartz, and S. Weinfurtner. Black Hole Quasibound States from a Draining Bathtub Vortex Flow. "Phys. Rev. Lett.", 121:061101, Aug, 2018.

[29] P. O. Fedichev and U. R. Fischer. "Cosmological" quasi-particle production in harmonically trapped superfluid gases. *Physical Review A*, 69(3):033602, 2004.

[30] C. Barcelo, S. Liberati, and M. Visser. Analogue models for frw cosmologies. *International Journal of Modern Physics D*, 12(09):1641–1649, 2003.

[31] S. Weinfurtner, P. Jain, M. Visser, and C. W. Gardiner. Cosmological particle production in emergent rainbow spacetimes. *Classical and Quantum Gravity*, 26(6):065012, 2009.

[32] P. Jain, S. Weinfurtner, M. Visser, and C. W. Gardiner. Analog model of a friedmann-robertson-walker universe in bose-einstein condensates: Application of the classical field method. *Physical Review A*, 76(3):033616, 2007.

[33] S.-Y. Chä and U. R Fischer. Probing the scale invariance of the inflationary power spectrum in expanding quasi-two-dimensional dipolar condensates. "Phys. Rev. Lett.", 118(13):130404, 2017.

[34] Uwe R. Fischer and Ralf Schutzhold. Quantum simulation of cosmic inflation in two-component Bose-Einstein condensates. *Phys. Rev. A*, 70:063615, 2004.

[35] J.-C. Jaskula, G. B. Partridge, M. Bonneau, R. Lopes, J. Ruaudel, D. Boiron, and C. I. Westbrook. Acoustic analog to the dynamical casimir effect in a bose-einstein condensate. "Phys. Rev. Lett.", 109(22):220401, 2012.

[36] S. Eckel, A. Kumar, T. Jacobson, I. B. Spielman, and G. K. Campbell. A supersonically expanding bose-einstein condensate: an expanding universe in the lab. *arXiv preprint arXiv:1710.05800*, 2017.

[37] K. A. Baldwin, M. M. Scase, and R. J. A. Hill. The inhibition of the Rayleigh-Raylor instability by rotation. *Scientific reports*, 5:11706, 2015.

[38] M. M. Scase, K. A. Baldwin, and R. J. A. Hill. The Rotating Rayleigh-Taylor instability. *arXiv:1603.00675*.

[39] M. V. Berry and A. K. Geim. Of flying frogs and levitrons. *European Journal of Physics*, 18(4):307, 1997.

[40] M. D. Simon and A. K. Geim. Diamagnetic levitation: flying frogs and floating magnets. *Journal of Applied Physics*, 87(9):6200–6204, 2000.

[41] L. D. Landau and E. M. Lifshits. *Fluid Mechanics: Transl. from the Russian by JB Sykes and WH Reid.* Addison-Wesley, 1959.

[42] P. W. G. Poodt, M. C. R. Heijna, P. C. M. Christianen, W. J. P. van Enckevort, W. J. de Grip, K. Tsukamoto, J. C. Maan and E. Vlieg. Using Gradient Magnetic Fields to Suppress Convection during Crystal Growth *Crystal Growth & Design* 6(10):2275–2280, 2006.

[43] J. W. Whalen. Physical chemistry of surfaces, fourth edition (adamson, arthur w.). *Journal of Chemical Education*, 60(11):A322, 1983.

[44] L. Liao and R. J. A. Hill. Shapes and fissility of highly charged and rapidly rotating levitated liquid drops. "Phys. Rev. Lett.", 119(11):114501, 2017.

[45] P. J. Cobelli, A. Maurel, V. Pagneux, and P. Petitjeans. Global measurement of water waves by Fourier transform profilometry. *Exp Fluids*, 46:1037, 2009.

[46] F. Moisy, M. Rabaud, and K. Salsac. A synthetic Schlieren method for the measurement of the topography of a liquid interface. *Exp Fluids*, 46:1021, 2009

[47] S. Wildeman. Real-time quantitative schlieren imaging by fast fourier demodulation of a checkered backdrop. *Exp Fluids*, 59:97, 2018.

[48] L. P. Grishchuk and Y. V. Sidorov. Squeezed quantum states in theory of cosmological perturbations. In *5th Seminar on Quantum Gravity Moscow, USSR, May 28-June 1, 1990*, pages 678–688, 1990.

[49] A. Albrecht, P. Ferreira, M. Joyce, and T. Prokopec. Inflation and squeezed quantum states. *Phys. Rev. D*, 50:4807–4820, 1994.

[50] N. D. Birrell and P. C. W. Davies. *Quantum Fields in Curved Space*. Cambridge Monographs on Mathematical Physics. Cambridge University Press, 1982.

[51] We split the field into the normalized eigenfunctions f_k and the quasi-particle amplitudes b_k to connect our derivation to the common literature on QFT in curved spacetime, although in our classical system both terms are c-numbers.

[52] V. Bacot, M. Labousse, A. Eddi, M. Fink, E. Fort. Time reversal and holography with spacetime transformations. *Nature Physics*, 12, 972–977, 2016.